Electronic Supplementary Material (ESI) for Materials Horizons.

Supporting Information

Engineering Viscoelastic Mismatch for Temporal Morphing of Tough Supramolecular Hydrogels

Xing Peng Hao[a,†], Chuan Wei Zhang[a,†], Wei Hong[b], Meng Meng[c], Li Xin Hou[a], Miao Du[a], Qiang Zheng[a], Zi Liang Wu[a,*]

[a] Ministry of Education Key Laboratory of Macromolecular Synthesis and Functionalization, Department of Polymer Science and Engineering, Zhejiang University, Hangzhou 310027, China;

[b] Department of Mechanics and Aerospace Engineering, Southern University of Science and Technology, Shenzhen 518055, China;

[c] Design Informatics, Edinburgh College of Art, University of Edinburgh, Edinburgh EH8 9JS, UK.

[†] These authors contributed equally to this work.

* Corresponding author. E-mail: wuziliang@zju.edu.cn

Experimental Section

Materials

Acrylamide (AAm), methacrylic acid (MAAc), methacrylamide (MAAm), potassium persulfate (KPS, initiator), sodium chloride (NaCl), and benzophenone were used as received from Aladdin Chemistry Co., Ltd. *N*,*N*,*N'*,*N'*-tetramethylethylenediamine (TMEDA) was purchased from Sigma-Aldrich Co., Ltd. Iron oxide particles (Fe_3O_4, 99.99%; mean diameter: 25 nm) was purchased from Alibaba Co., Ltd. Laponite clay (Laponite XGL) was purchased from Guangzhou Bofeng Chemical Co., Ltd. Polydimethylsiloxane (PDMS; Sylgard 184) was purchased from Dow Corning Co., Ltd. VHB tape was purchased from 3M Co., Ltd. Millipore deionized water was used in all the experiments.

Preparation of singular and bilayer hydrogel sheets

The tough supramolecular hydrogels were facilely prepared by polymerization of the aqueous precursor solutions. The poly(MAAm-*co*-MAAc) (MM) hydrogel and poly(AAm-*co*-MAAc) (AM) hydrogel were synthesized by free-radical copolymerization of monomers.[S1] Prescribed amounts of monomers, KPS (0.5 mol%, relative to total monomers), and TMEDA (0.1 vol%, relative to total volume) were dissolved in water (Table S3). The obtained precursor solution was injected into a reaction cell consisting of a pair of glass substrates separated with a silicone spacer (thickness: 1 mm), which was kept in an oven of 45 ^{o}C for 8 h to complete the polymerization. The as-prepared hydrogels were swelled in large amount of water to remove the residuals and achieve the equilibrium state. To prepare the bilayer hydrogel, the equilibrated MM hydrogel sheet with thickness of ~1 mm was used as one substrate for the synthesis of AM hydrogel. A new reaction cell was assembled with MM gel on one glass substrate and 2 mm-thick silicone spacer. After the precursor solution of AM hydrogel was injected into the reaction cell and polymerized at 45 ^{o}C for 8 h. The as-prepared bilayer hydrogel was then equilibrated in large amount of water. The resultant bilayer hydrogels were cut into desired shape by a laser cutter (BSCK, BCL-6325). Corresponding dimensions of the hydrogels for temporal morphing are shown in Fig. S17.

Characterizations of the tough supramolecular hydrogels

To test the mechanical properties of AM and MM hydrogels, dumbbell-shaped samples with a width of 2 mm and a gauge length of 12 mm were cut from the planar hydrogel sheets. The mechanical properties were measured by using a commercial tester (Instron 3343) at room temperature with a constant stretching rate of 100 mm min^{-1}. Young's modulus of the hydrogel was calculated from the tensile stress-strain curve below a strain of 5%. The viscoelasticity of the gels was characterized by using a DHR-2 rheometer (TA Instruments). Disk-like gels with a diameter of 25 mm were placed between the parallel plates of the rheometer. The periphery of the sample was sealed with liquid wax to reduce the solvent evaporation from the hydrogel. Temperature-sweep measurement (heating rate: 5 ^{o}C min^{-1}) was performed to the hydrogel sample with a frequency of 1 Hz and a strain amplitude of 0.05%. The glass transition temperature, T_g, was extracted from the peak value of loss factor tan δ of the dynamic spectra.

T_g of the hydrogels equilibrated in saline solutions was examined by dynamic mechanical analysis (DMA) in single cantilever beam mode using DMA Q800 equipment (TA Instruments). The gels previously equilibrated in saline solutions with different concentrations of NaCl (C_{NaCl}) for 24 h were cut into rectangular strips with dimensions of 17.5 mm × 12.7 mm × 1 mm. The surface of the sample was covered with liquid wax to prevent the solvent evaporation. The spectra of tan δ' were obtained by temperature-sweep from 0 to 80 ^{o}C with a frequency of 1 Hz and a heating rate of 5 ^{o}C min^{-1}.

To characterize the plastic deformation of AM hydrogel that was treated with 2 M saline solution at specific sites, the resultant hydrogel was stretched to 100% strain and the birefringence of the hydrogel was observed under a polarizing optical microscope (Nikon, LV100N POL) with and without the 530 nm tint plate.

Programmed temporal morphing of bilayer and singular hydrogels

For temporal morphing of the bilayer hydrogels with or without kirigami structures, the pre-stretching was imposed on the gels with prescribed mechanical strain at certain stretching rate under specific temperature. The external force was removed after a short holding period or immediately after the pre-stretch; morphing process of the gel was recorded by a digital camera (Sony A7M3).

For the programmed morphing of the bilayer hydrogel, the viscoelasticity modulation was realized by site-specific saline treatment to locally tailor the glass transition temperature of both AM and MM gels. Perforated pattern was created in the transparency of polyethylene terephthalate (PET) by a laser cutter;

which was used to direct the saline treatment at specific regions of the hydrogel. Before or after pre-stretching, the bilayer gel was sandwiched by a pair of perforated masks and followed by spraying of the saline solution (2 M NaCl solution) to regulate the local viscoelasticity of the gel. Temporal morphing of the gel took place after removal of the external force. The bilayer hydrogel with viscoelasticity gradients recovered its original shape after being transferred into water to dialyze out the salts. The identical hydrogel can be reprogrammed to other configurations by saline treatments with different masks.

Programmed morphing of singular hydrogel was realized by the similar regulation strategy. After pre-stretching, AM hydrogel was sandwiched by a pair of perforated masks followed by site-specific saline treatment (2 M NaCl solution) for a certain period of time to locally tailor the viscoelasticity of the gel. The singular gel with transient gradients also showed temporal morphing after release from the pre-stretch. The dimensions of AM hydrogels and corresponding masks used for saline treatment are shown in Fig. S18.

Fabrication of tough hydrogel-based magnetic soft robots

To prepare the magnetic soft robots, 8 wt% (relative to total weight of the gel) of Fe_3O_4 nanoparticles and 5 wt% of laponite clays were added into the precursor solutions of AM and MM gels followed with ultrasound treatment for 10 min. Other procedures to prepare the bilayer hydrogel and singular AM hydrogel are the same as described above. The hydrogels were cut into desired shapes as magnetic soft robots and equilibrated in 1 M or 2 M saline solution to further regulate the viscoelasticity. Magnetic soft robots with temporal 3D configurations were obtained by uniaxial or biaxial stretching of the hydrogel sheets. To locally control the shape change and shape recovery of the hydrogel, 520 nm laser light (intensity: 7 W cm^{-2}) was used to regulate the local temperature of the gel. The variation of the temperature was recorded by a thermal imager (FOTRIC 280). Locomotion of the soft robots with different gaits was steered by a moving permanent magnet (magnetic strength: 25 mT; dimensions: 50 mm × 30 mm × 15 mm) below the soft robots with a distance of ~50 mm. The locomotion behavior was recorded by a digital camera with a cut-off filter (600-1100 nm).

Integration of temporal morphing hydrogels with elastomers

Hybrid material of AM hydrogel and PDMS was developed according to the reported protocol.[S2] The precursor of PDMS has two components: a base (part A) and a cure agent (part B). Briefly, 0.3 wt% (relative to the mass of part A) of benzophenone was added into part A and heated to 60 °C for 2 h. After the mixture was cooled down to room temperature, 10 wt% (relative to the mass of part A) of part B was added. Air bubbles in the viscous solution were removed by placing it in a vacuum desiccator. The precursor was transferred into a reaction cell and placed at room temperature for 2 h. Then, the precursor solution of AM hydrogel was poured on the semi-cured PDMS and kept for another 2 h in 45 °C oven. The sample was placed under 365 nm UV light for 6 h to form robust interfacial bonding between AM gel and PDMS elastomer. The sample was then kept in 45 °C oven for another 6 h to complete the polymerization. For AM hydrogel and VHB tape, the two materials were integrated by simple pressing. Programmed temporal morphing of the hybrid materials with distinct viscoelasticity was realized by pre-stretching and releasing.

Theoretical analysis and numerical modeling of temporal morphing behavior

To simulate the temporal morphing of the viscoelastic gels, we insert the materials model described above into the general framework of continuum mechanics, and solve the equation of mechanical equilibrium

$$\nabla \cdot s = 0, \#(S1)$$

together with the definition of the deformation gradient

$$F_{iK}^{0\to t} = \frac{\partial x_i(X,t)}{\partial X_K} \#(S2)$$

and the constitutive relation (Eq. (1) in the main text). Here $x(X,t)$ is the coordinate of a material particle, which is located at X when $t = 0$. Inertia and body forces are neglected. The nonlinear partial differential equations are solved by using a finite element method through customized modules in the commercial package COMSOL Multiphysics.

Instead of integrating the convoluted expression (Eq. (1)), in which the entire deformation history needs to be stored, we differentiate the Cauchy stress $\sigma^{(i)}$ from the i^{th} Prony component and write its rate of change as:

$$\dot{\sigma}^{(i)} = kT\rho(t)\frac{\alpha_i}{\tau_i}I - \frac{\sigma^{(i)}}{\tau_i} + L\cdot\sigma^{(i)} + \sigma^{(i)}\cdot L^T. \#(S3)$$

The right-hand side of Eq. (S3) depends only on the quantities that can be evaluated at the current time. We therefore integrate Eq. (S3) at every time step to update and store the Prony stress components over Gauss point, and then combine them with the regular stress-analysis procedures to calculate the field of deformation and simulate the temporal morphing of the gel structures. In the numerical calculation, linear brick elements are used for the displacements, and the Prony stress components are calculated and stored on the single Gauss point in each element. The implicit BDF (backward differentiation formula) method is used for time integration.

In the simulations, the samples are gradually loaded to certain nominal strains according to the corresponding experiments, and then quickly released (within 0.01 s) to see the temporal evolution. While switching from a displacement boundary condition (loading) to a traction boundary condition (unloading) is unavailable in COMSOL, we employ a weak boundary condition to connect the boundaries to a control point with a variable stiffness link, whose stiffness decreased from the initial high value (for rigid connection) to zero within the releasing interval. Symmetry of the structures has been fully exploited to reduce the computational cost.

The viscoelastic properties of the hydrogels are significantly altered by the glass transition. While the underlying physics associated with the glass transition process has been studied and accurate rheological changes extensively characterized in the literature,[S3] here for the purpose of designing and illustrating the actuation mechanisms, we model the glass transition of the hydrogels simply by increasing the formation rate of subnetworks, and write it into a function of time, $\eta(t)$. The value of η at a glassy state is taken from the measured modulus values, and a smooth ramping function is adopted to model the transition.

References

S1 C. Du, X. N. Zhang, T. L. Sun, M. Du, Q. Zheng and Z. L. Wu, *Macromolecules*, 2021, **54**, 4313-4325.

S2 Y. J. Wang, X. N. Zhang, Y. Song, Y. Zhao, L. Chen, F. Su, L. Li, Z. L. Wu and Q. Zheng, *Chem. Mater.*, 2019, **31**, 1430-1440.

S3 H. Yang, C. Li, M. Yang, Y. Pan, Q. Yin, J. Tang, H. J. Qi and Z. Suo, *Adv. Funct. Mater.*, 2019, **29**, 1901721.

S4 J. D. Ferry, *Viscoelastic properties of polymers.* John Wiley & Sons, New York, 1980.

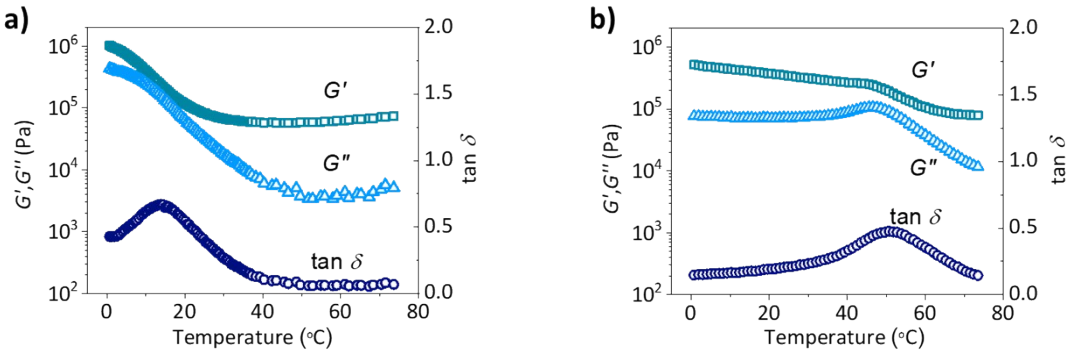

Fig. S1. Temperature sweep spectra of storage modulus *G′*, loss modulus *G″*, and loss factor tan *δ* of AM gel (a) and MM gel (b) from 0 to 75 °C at a frequency of 1 Hz and a strain amplitude of 0.05%. Heating rate: 5 °C min^{-1}.

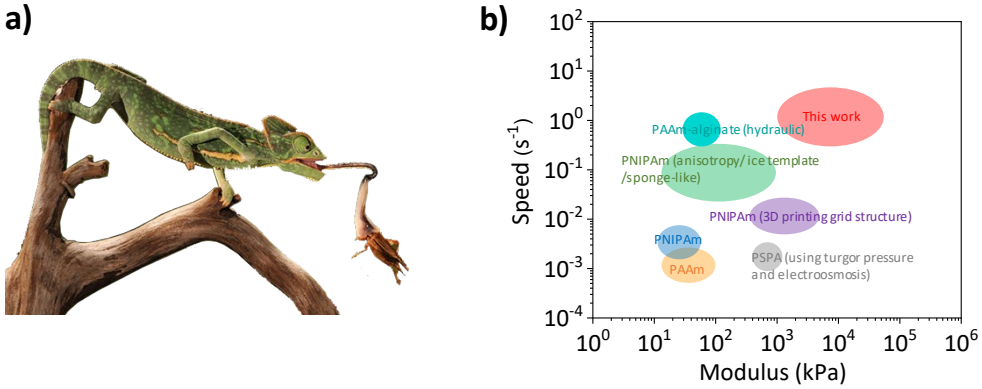

Fig. S2. (a) Rapid deformation of chameleon's tongue for catching insects. (b) Comparison of Young's modulus and deformation speed of hydrogel materials by viscoelasticity-induced morphing in this work and other osmatic-pressure-driven deformations.[S5-S11] The speed is defined by the reciprocal of the time that is needed to complete the prescribed deformation. PAAm: polyacrylamide; PSPA: poly(3-sulfopropylacrylate) potassium salt.

References

S5 X. P. Hao, Z. Xu, C. Y. Li, W. Hong, Q. Zheng and Z. L. Wu, *Adv. Mater.*, 2020, **32**, 2000781.

S6 Y. S. Kim, M. Liu, Y. Ishida, Y. Ebina, M. Osada, T. Sasaki, T. Hikima, M. Takata and T. Aida, *Nat. Mater.*, 2015, **14**, 1002-1007.

S7 Y. Zhao, C.-Y. Lo, L. Ruan, C.-H. Pi, C. Kim, Y. Alsaid, I. Frenkel, R. Rico, T.-C. Tsao and X. He, *Sci. Robot.*, 2021, **6**, eabd5483.

S8 S. Y. Zheng, Y. Shen, F. Zhu, J. Yin, J. Qian, J. Fu, Z. L. Wu and Q. Zheng, *Adv. Funct. Mater.*, 2018, **28**, 1803366.

S9 Y. Alsaid, S. Wu, D. Wu, Y. Du, L. Shi, R. Khodambashi, R. Rico, M. Hua, Y. Yan, Y. Zhao, D. Aukes and X. He, *Adv. Mater.*, 2021, **33**, 2008235.

S10 H. Yuk, S. Lin, C. Ma, M. Takaffoli, N. X. Fang and X. Zhao, *Nat. Commun.*, 2017, **8**, 14230.

S11 H. Na, Y.-W. Kang, C. S. Park, S. Jung, H.-Y. Kim and J.-Y. Sun, *Science*, 2022, **376**, 301-307.

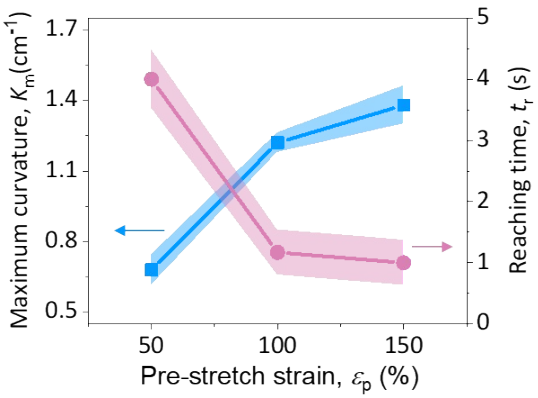

Fig. S3. Maximum curvature, K_m, and the time required to reach K_m, t_r, of the bilayer gel with different pre-stretch strain, ε_p. This graph was summarized from Fig. 1j. The mean (solid line) and standard deviation (shaded area) are from three independent experiments.

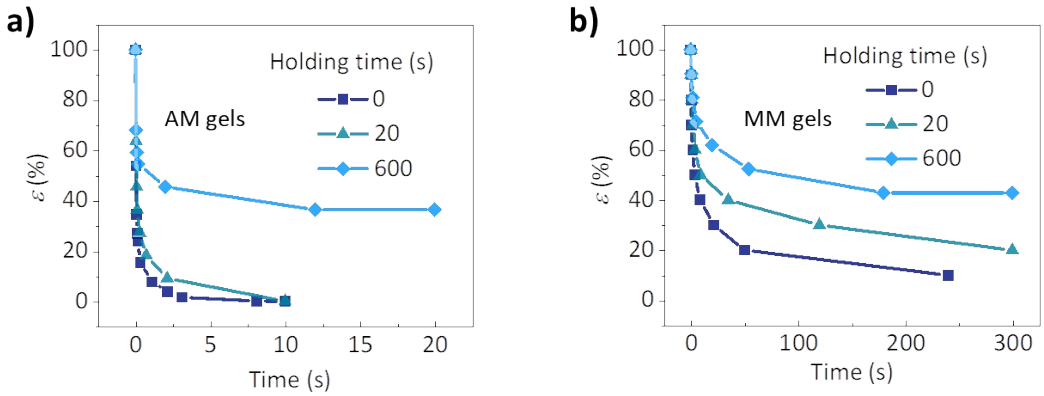

Fig. S4. Residual strain (ε) of AM gel (a) and MM gel (b) during the recovery process after pre-stretching (strain, 100%) with different holding time. Temperature, 20 °C.

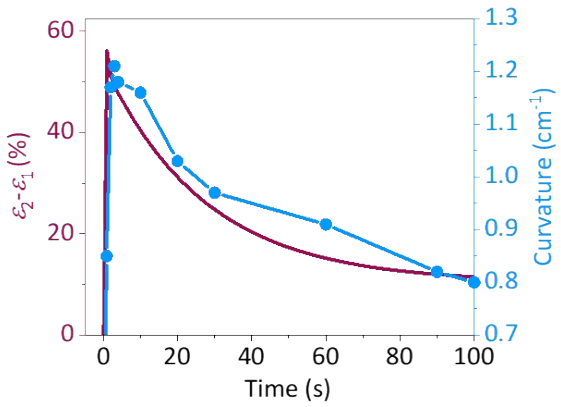

Fig. S5. Relationship between the differential residual strain (ε) of MM and AM gels and the curvature of the bilayer hydrogel. Differential residual strain ($\varepsilon = \varepsilon_2 - \varepsilon_1$) was measured by subtracting the residual strain of AM gel (ε_1) from that of MM gel (ε_2). The curvature of the bilayer hydrogel at different recovery time was measured during the recovery process after pre-stretching (strain, 100%). Temperature, 20 °C; holding time, 0 s.

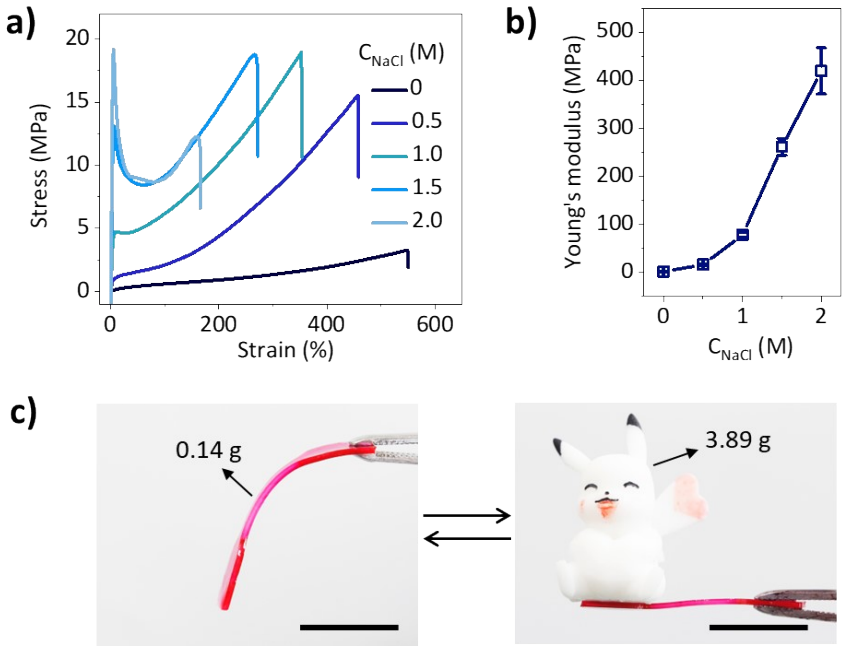

Fig. S6. (a) Tensile strain-stress curves of AM gels after being incubated in saline solutions with different concentration of NaCl (C_{NaCl}) for 24 h. (b) Variations of Young's modulus of AM gels as a function of C_{NaCl}. Error bar represents the standard deviation of the mean (n = 3). (c) Photos to demonstrate the varied stiffness of the AM gel before (left) and after (right) the saline treatment (C_{NaCl} = 2 M). Scale bars, 1 cm.

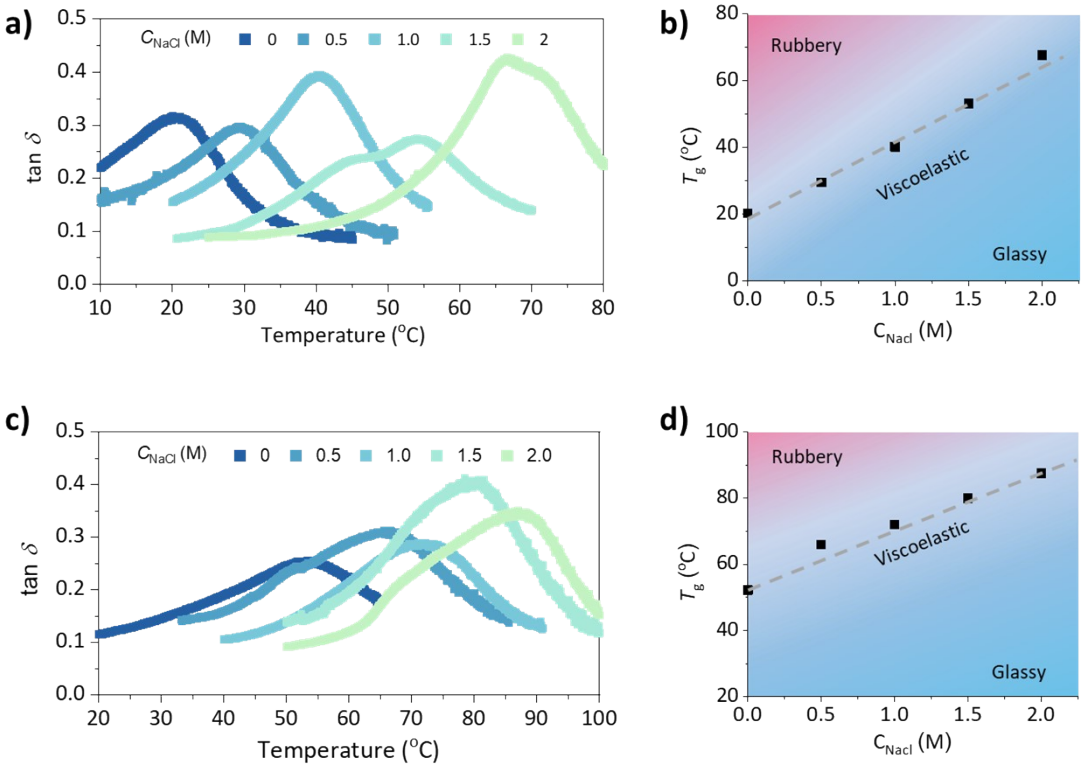

Fig. S7. (a,c) Loss factor tan δ of AM gels (a) and MM gels (c) after being equilibrated in saline solutions with different concentrations (C_{NaCl}) for 24 h. Frequency, 1 Hz; strain amplitude, 0.05%; heating rate, 5 °C min^{-1}. (b,d) Variations of T_g of AM gels (b) and MM gels (d) as a function of saline concentrations.

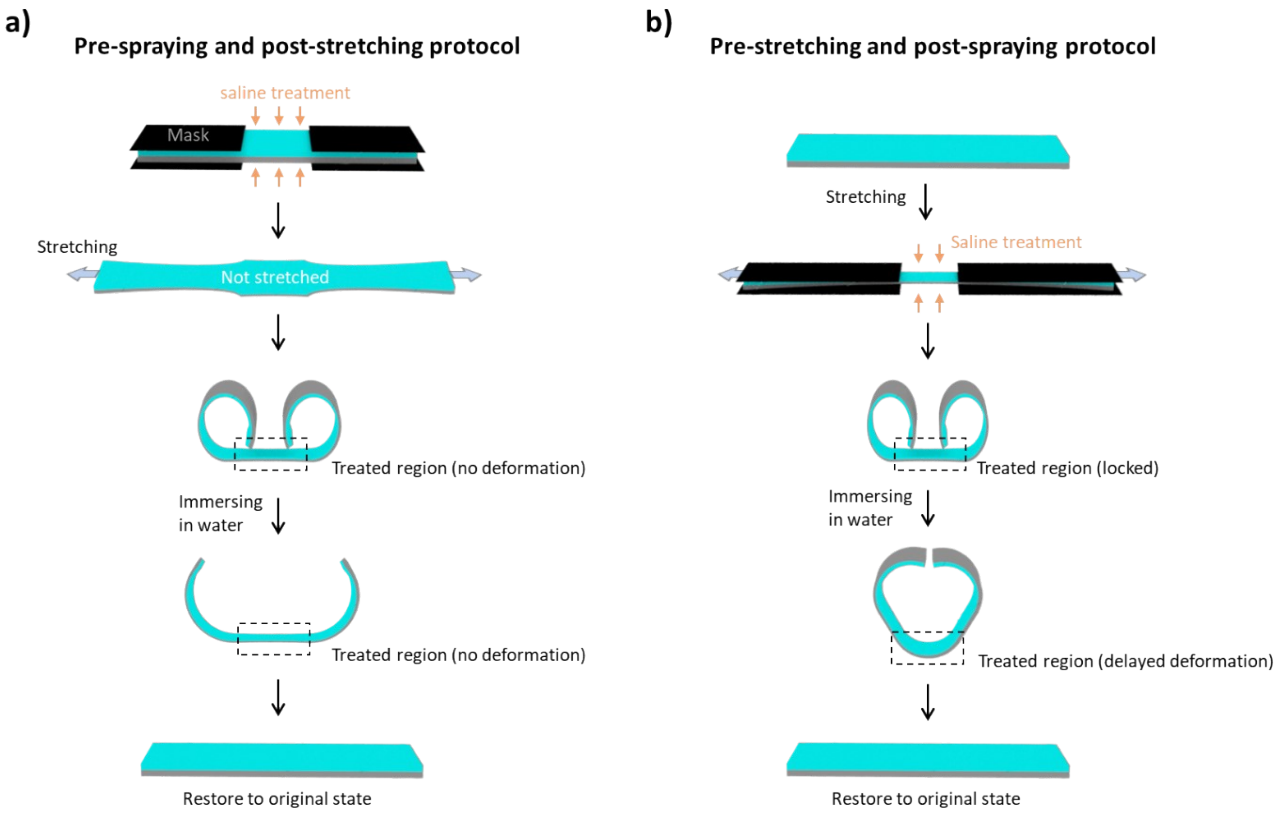

Fig. S8. Schematic to show the different regulation strategies and corresponding morphing behaviors of the bilayer gel strips with engineered viscoelastic mismatch: (a) Pre-spraying and post-stretching; (b) pre-stretching and post-spraying.

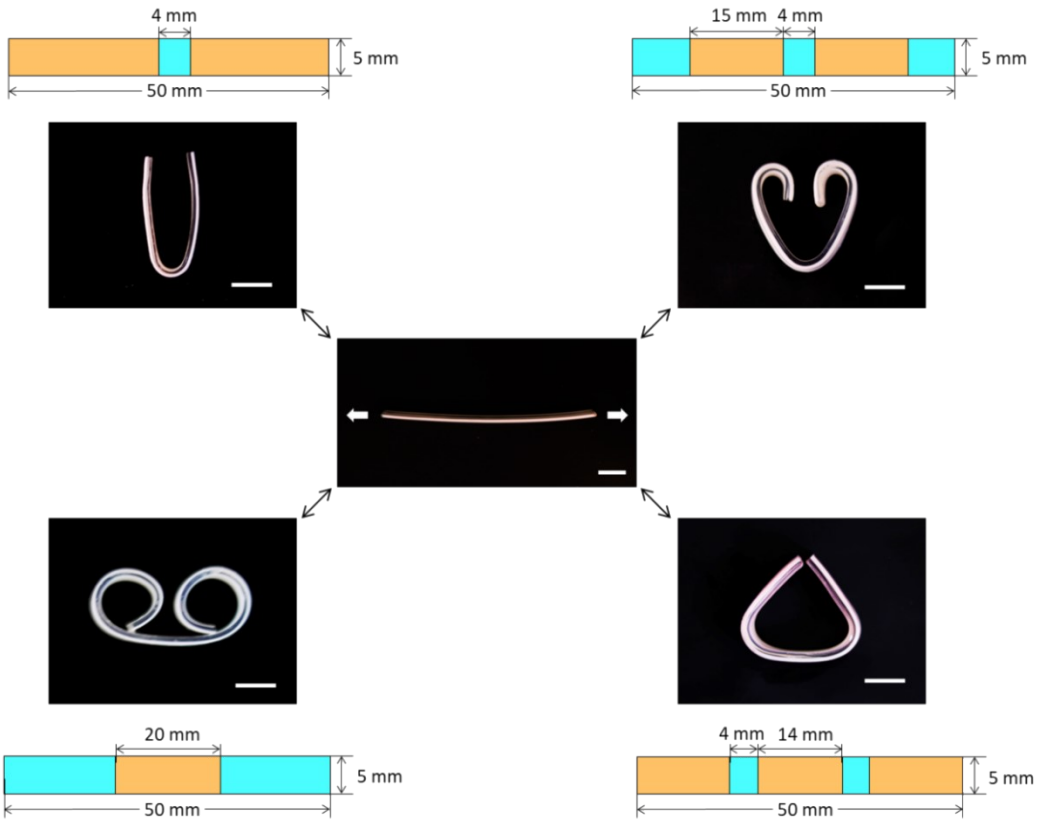

Fig. S9. Various configurations obtained from one hydrogel strip through site-specific saline treatment. The photos were taken during the temporal morphing process. The schemes present the dimensions of the bilayer hydrogel strip and the locations (light blue regions) for the saline treatment from both sides before pre-stretching. The white arrows indicate the pre-stretch directions. Scale bars, 1 cm.

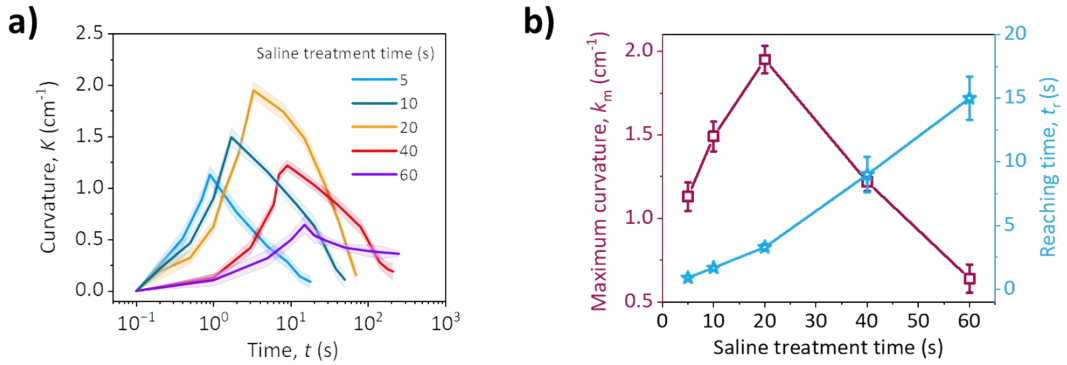

Fig. S10. (a) Varying curvature of singular AM gel during the morphing process at room temperature after pre-stretching to 100% strain, saline treatment for a certain period of time, and then immediate release from pre-stretch. The slender AM gel is treated by 2 M NaCl solution from one side, which tailors the viscoelasticity and reduces the recovery speed of the treated layer after the pre-stretch and release step. (b) Maximum curvature, K_m, and the time required to reach K_m, t_r, of the AM gel with different saline treatment time. The mean and standard deviation are from three independent experiments. Dimensions of AM gel, 50 mm × 10 mm × 1 mm.

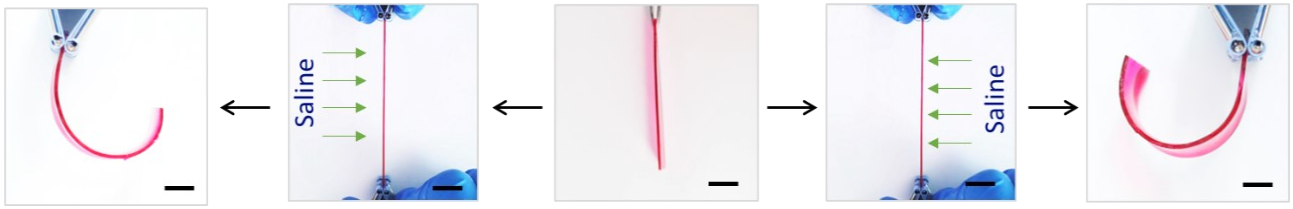

Fig. S11. Bidirectional deformation of the singular hydrogel. Saline concentration, 2 M; treatment time, 20 s. Scale bars, 1 cm.

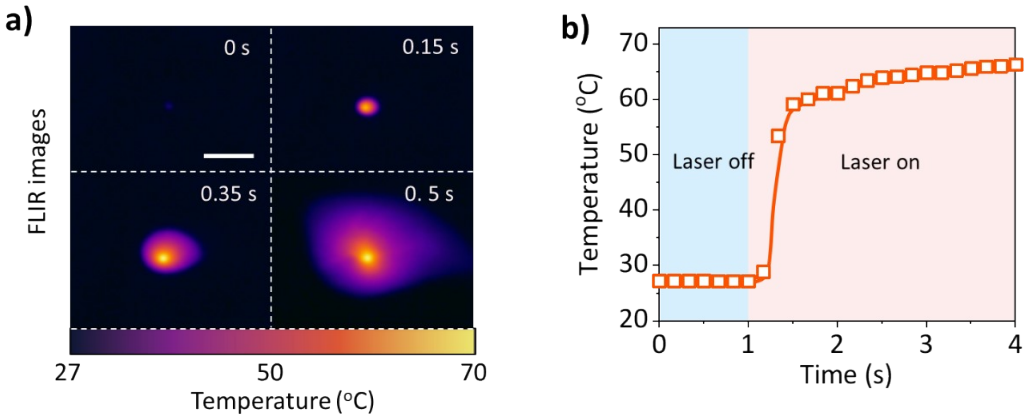

Fig. S12. (a) Forward-looking infrared (FLIR) imagers of AM gel containing Fe_3O_4 nanoparticles under the irradiation of a laser (wavelength, 520 nm; intensity, 7 W cm^{-2}). Scale bar, 1 cm. (b) Variation of the central point temperature of the irradiated area as a function of irradiation time.

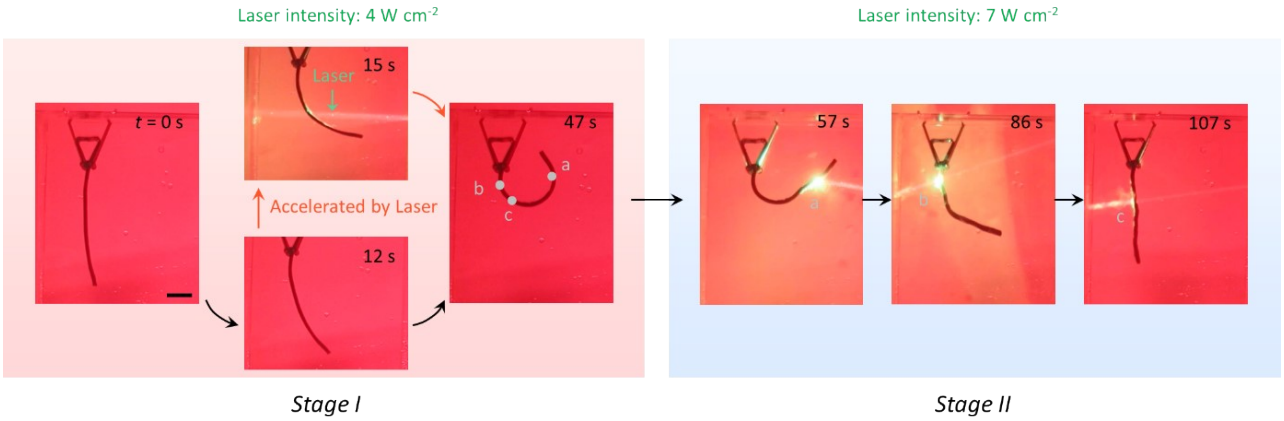

Fig. S13. Laser-regulated shape-morphing of the bilayer hydrogel in the saline solution. The bilayer hydrogel containing Fe_3O_4 nanoparticles was previously equilibrated in 1 M saline solution. As shown in Fig. S7b and S7d, T_g of AM gel and MM gel in 1 M saline solution are 40 °C and 72 °C, respectively. At room temperature, AM gel recovered slowly (due to the broad glass transition), but MM gel cannot. Thus, the bilayer gel gradually deformed into an arch after pre-stretch (Stage I). This process can be accelerated by light irradiation. When irradiated with a low-intensity laser (4 W m^{-2}), the local temperature rose to ~40 °C within 1 s, resulting in promoted self-recovery of AM gel rather than MM gel. The local morphing speed of the bilayer gel was expedited, but the final configuration of stage I (i.e. an arc shape) did not change, which was determined by the elastic energy stored in AM gel. In stage II of the shape recovery process, a high-intensity laser (7 W m^{-2}) was applied to raise the local temperature to ~65 °C, which was close to T_g of MM gel. At this condition, MM gel showed fast recovery under laser irradiation, but remained static without the irradiation. Laser irradiation was highly efficient to regulate the permanent configurations in stage II. Scale bar, 1 cm.

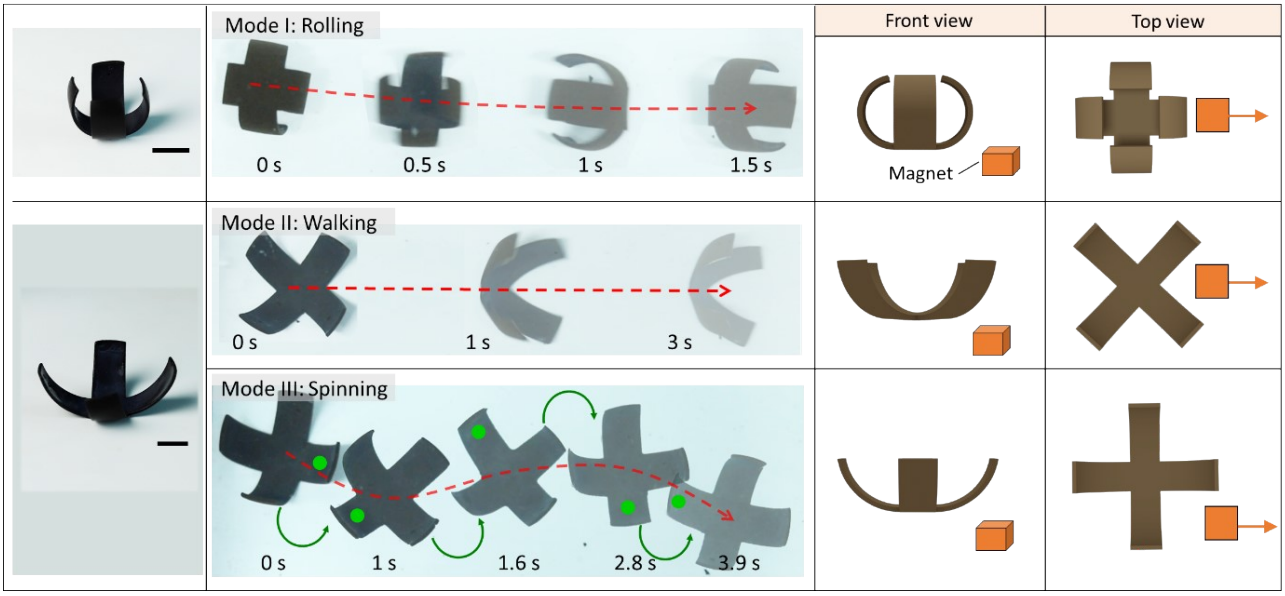

Fig. S14. Multimode locomotion of hydrogel-based magnetic robot with selectively fixed temporal configurations. The configurations of the cross-shaped hydrogel robot were fixed on demand during the temporal morphing process by transferring it to 2 M saline solution. The magnetic hydrogel robot showed rolling, walking, and spinning motion modes, depending on the fixed configuration and the applied magnetic field. The red dash arrows indicate the motion direction and the path of the magnetic robot. The green arrows indicate the spinning directions of the hydrogel, and the green dot is a reference mark to show the spinning motion. The right two columns show the schematics of temporal configurations and the position of the magnet relative to the gel robot. The orange arrows indicate the moving direction of the magnet. The permanent magnet (dimensions: 50 mm × 30 mm × 15 mm) was applied under the hydrogel robot with a distance of ~50 mm, and the magnetic strength is ~25 mT. Scale bars, 1 cm.

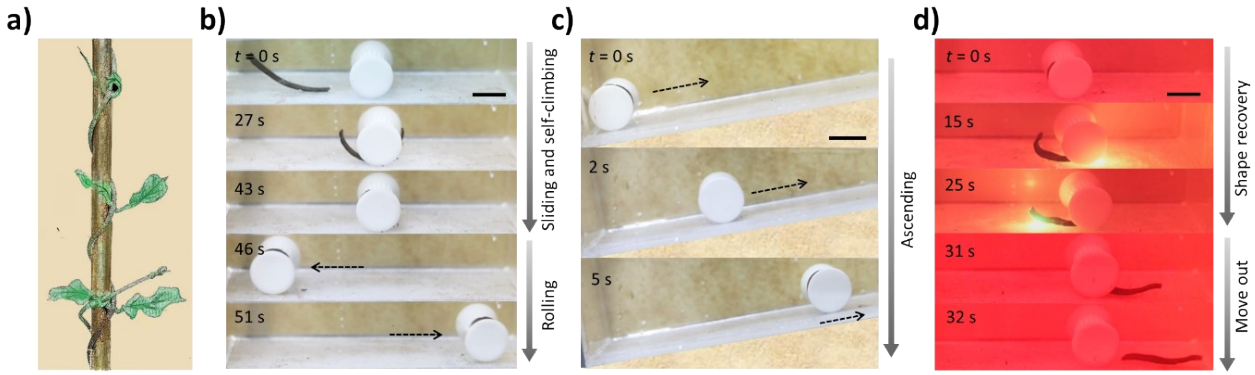

Fig. S15. (a) Schematic of living twining plant parasitized on dead branch. (b-d) Pre-stretched bilayer hydrogel strip self-warped on a polyester pillar to afford mobility to roll (b) and climb on a slope (c). The gel strip was removed from the pillar by laser-mediated shape recovery and magnet-directed sliding away (d). Scale bars, 1 cm.

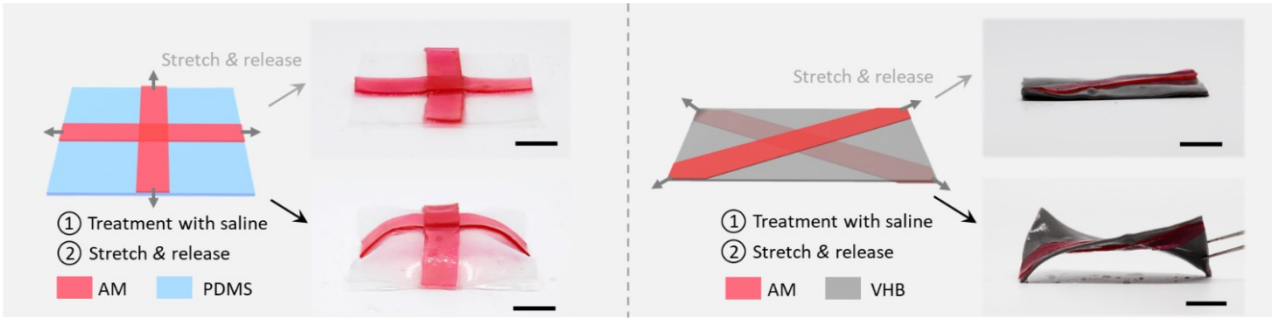

Fig. S16. Generality of viscoelasticity-induced temporal shape morphing to other elastic materials. Temporal configurations of elastomer-hydrogel hybrids obtained by harnessing the viscoelastic mismatch. AM gel was highly viscoelastic, whereas polydimethylsiloxane (left) and VHB tape (right) were elastic. According to the incubation time of the hybrid materials in saline solution, the resultant configurations after pre-stretching were flat, temporal, and permanent, respectively. Scale bars, 1 cm.

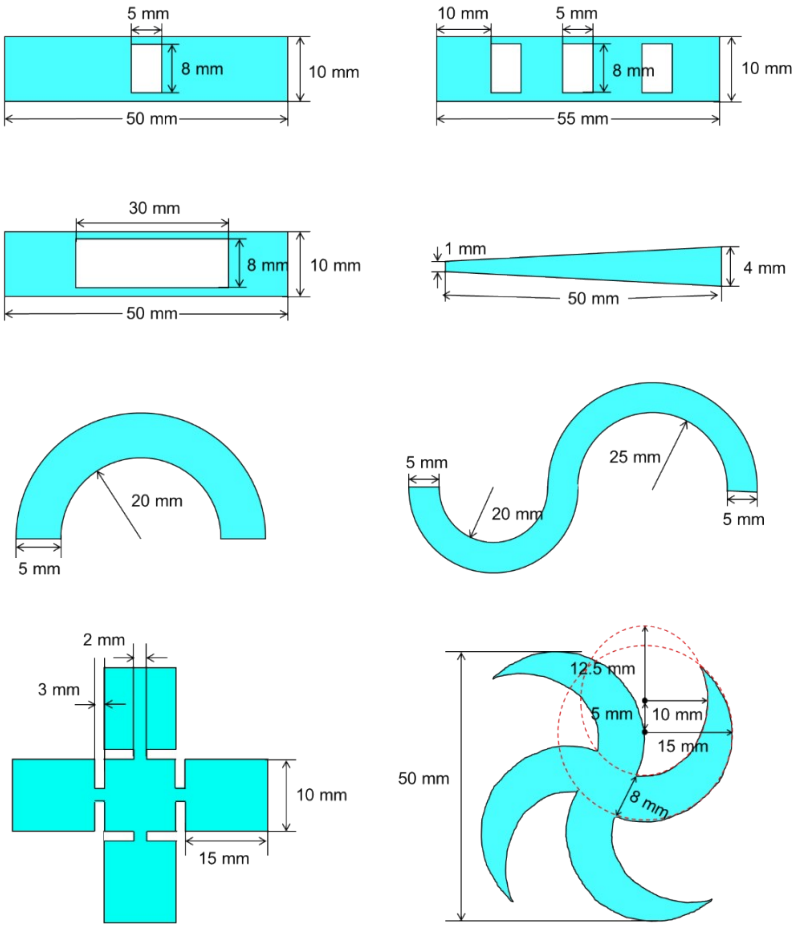

Fig. S17. Dimensions of the hydrogel sheets in Fig. 3.

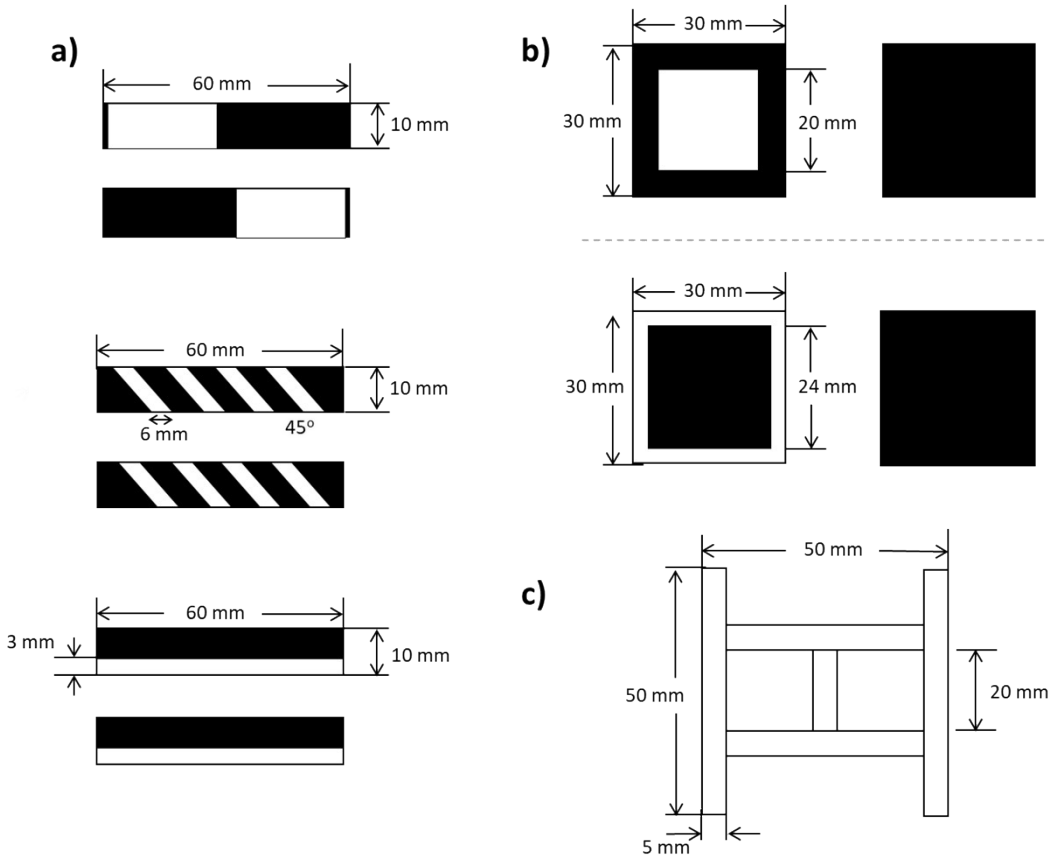

Fig. S18. (a,b) Dimensions of the masks and the hydrogels for site-specific saline treatment in Fig. 4a and 4b. The black parts in (a) and (b) represent the locations that were covered by the masks from the upper and bottom sides of the gel, and the white parts were the locations that were treated with saline solutions. (c) Dimensions of the hydrogel in Fig. 4d.

Table S1. Prony series fitting parameters to the stress-relaxation tests at 20 °C.

i	AM gel		MM gel	
	α_i	τ_i **(s)**	α_i	τ_i **(s)**
0	0.250	–	0.050	–
1	0.262	0.168	0.489	0.119
2	0.156	2.85	0.197	1.67
3	0.119	72.9	0.132	22.2
4	0.213	656	0.133	539

Table S2. Summary and comparison of different regulation methods used in this work for viscoelasticity-mediated temporal morphing of tough gels.

System	Regulation strategy	Resulted effects		Feature	Advantage	Demonstration
		After stretching	After-releasing			
Bilayer (AM+MM) gel	1) spaying of saline; 2) pre-stretching; 3) release from stretching	Treated region: stiffened yet not stretched; Untreated region: stretched	Treated region: no morphing; Untreated region: temporal morphing	Temporal deformation only in untreated region	Spontaneous morphing and recovery	Fig. 3e & Fig. 3g
	1) pre-stretching; 2) spaying of saline; 3) release from stretching; 4) immersion in water	Treated region: stiffened and stretched; Untreated region: stretched	Treated region: no morphing, until placed in water; Untreated region: temporal morphing	Temporal deformation in untreated region; delayed deformation in treated region after placed in water	Delayed temporal morphing [a]	Fig. 3f & Fig. 3h
	1) saline treatment; 2) pre-stretching; 3) release from stretching; 4) laser irradiation	The gel uniformly stiffened and stretched [b]	The gel partially recovered with a low speed, which is drastically accelerated by laser irradiation	Fast deformation in irradiated regions; slow recovery in untreated region	Remote and local control	Fig. 5b-5h & Fig. S13
Singular (AM) gel	1) pre-stretching; 2) post-spraying	Treated region: stiffened yet not stretched; Untreated region: stretched	Treated region: no morphing; Untreated region: temporal morphing	Temporal deformation only in untreated region	Selective bending direction [c]	Fig. 4

[a] After the gel is immersed in water, the stored elastic energy in the treated region will be released, resulting in delayed temporal deformation and shape recovery of this part.

[b] Both sides of the bilayer gel are treated by saline solution, leading to increase in T_g and decrease in the viscoelastic recovery speed.

[c] The bending direction of AM gel depends on which side treated by saline solution before release from pre-stretching.

Table S3. Recipes of precursor solutions for the synthesis of AM and MM gels.

Hydrogels	AAm (g)	MAAm (g)	MAAc (g)	H_2O (g)	KPS (g)	TMEDA (μL)
AM-0.25-6 [a]	2.132	–	7.748	9.958	0.162	200
MM-0.15-5 [b]	–	1.276	7.318	11.287	0.135	200

[a] The hydrogel of AM-0.25-6 indicates that the total monomer concentration (C_m) of AM gel is 6 M, and the feeding molar fraction of AAm (f_{AAm}) is 0.25.

[b] The hydrogel of MM-0.15-5 indicates that the total monomer concentration (C_m) of MM gel is 5 M, and the feeding molar fraction of MAAm (f_{MAAm}) is 0.15.

Movie S1. Illustration of the concept of viscoelasticity-induced temporal morphing of the bilayer hydrogel. Two trapezoid-shaped slender hydrogel strips with different viscoelasticity are combined into a bilayer structure. After pre-stretching, the different recovery speeds of the two gels result in strain/stress mismatch and thus temporal shape morphing of the bilayer gel.

Movie S2. Viscoelasticity-induced temporal morphing of a bilayer hydrogel for autonomously grabbing and releasing of an object at a constant condition. Half of the bilayer hydrogel strip was stretched to a strain of 50% and then incubated in 2 M saline solution for 3 min to suppress the recovery of the hydrogel. Temporal morphing was activated by immersing the bilayer hydrogel in water to dialyze out the salts. The hydrogel deformed into a hook to grab the printed plastic basket, and then recovered the flat shape to release the basket.

Movie S3. Laser-regulated temporal morphing of the bilayer hydrogel in saline solution. A bilayer hydrogel previously equilibrated in 1 M saline solution was pre-stretched to a strain of 50%. After the removal of external force, the hydrogel slowly curled into an arch at room temperature, which can be accelerated by laser irradiation to raise the local temperature of the hydrogel strip. The recovery process of the hydrogel was regulated by irradiation of a high-power laser to trigger the recovery of MM gel and thus the unbending of the bilayer gel.

Movie S4. Multimode locomotion of the hydrogel-based magnetic robot with desired temporal configurations. The cross-shaped bilayer hydrogel robot containing magnetic nanoparticles showed rolling, walking, and spinning gaits, depending on the configuration of the hydrogel and the magnetic field for actuation. The pre-stretched hydrogel was incubated in 2 M saline solution to suppress the shape recovery, which was triggered by transferring the gel to water for a period of time. The temporal configuration of the gel was fixed again in 2 M saline solution, which facilitated the locomotion under appropriate magnetic actuation.

Movie S5. Laser-regulated temporal morphing of magnetic hydrogel robot for cargo delivery. The cross-shaped soft robot made of bilayer hydrogel was previously equilibrated in 1 M saline solution, which gradually deformed into sphere-like configuration after the pre-stretch, enabling self-grabbing of the cargo. The hydrogel robot delivered the cargo to the destination by rolling under magnetic navigation. The cargo was released from the magnetic robot by laser-mediated shape recovery of one arm of the hydrogel. The hydrogel robot returned to its original location by rolling under the magnetic field.

Movie S6. Temporal morphing of magnetic hydrogel afforded inanimate object with motion ability. In 1 M saline solution, the pre-stretched bilayer hydrogel strip containing magnetic nanoparticles self-climbed to a polyester pillar, which became responsive to the magnetic field. The pillar showed rolling and ascending abilities under magnetic navigation. The magnetic gel can be removed from the pillar by laser irradiation to trigger the shape recovery process.